PCCP

PAPER

View Article Online
View Journal | View Issue

Cite this: *Phys. Chem. Chem. Phys.*, 2018, **20**, 22148

Effect of alkali ions on optical properties of flavins: vibronic spectra of cryogenic M^+lumichrome ions (M = Li–Cs) in the gas phase†

Pablo Nieto,[a] David Müller,[a] Alexander Sheldrick,[a] Alan Günther,[a] Mitsuhiko Miyazaki [ab] and Otto Dopfer *[a]

Received 21st June 2018,
Accepted 6th August 2018

DOI: 10.1039/c8cp03950j

rsc.li/pccp

The photochemical properties of flavins depend sensitively on their environment and are strongly modified by coordination with metal ions. Herein, the electronic spectra of cold complexes of the smallest flavin molecule (lumichrome, LC, $C_{12}N_4O_2H_{10}$) with alkali ions (M^+LC, M = Li–Cs) are measured by photodissociation in the visible range (VISPD) in a cryogenic ion trap coupled to a tandem mass spectrometer and an electrospray ionization source. The observed vibronic spectra of all ions are assigned to the optically bright $S_1 \leftarrow S_0$ ($\pi\pi^*$) transition of the most stable O4 isomer of M^+LC by comparison with quantum chemical calculations at the PBE0/cc-pVDZ level coupled to multidimensional Franck–Condon simulations. The rich vibronic spectra indicate substantial geometry changes upon S_1 excitation. Large red shifts of the S_1 origins upon metal complexation and progressions in the intermolecular in-plane metal stretch and bend modes demonstrate that the strength of the metal–flavin interaction in M^+LC(O4) strongly increases by S_1 excitation. The stronger $M^+\cdots$LC bond in the S_1 state of M^+LC(O4) is rationalized by the charge reorganization upon $\pi\pi^*$ excitation of the LC chromophore. The computations confirm that the optical properties of LC can be strongly modulated by metalation *via* both the type and binding site of the metal ion.

1. Introduction

Flavins are yellow bioorganic dye molecules derived from the heterocyclic 7,8-dimethyl-10-alkylisoalloxazine chromophore (iso-lumichrome = iso-LC = $C_{12}N_4O_2H_{10}$, R = H at N10, Fig. 1). The most fundamental members of the flavin family are lumichrome (LC, no substituent at N10 but H at N1), lumiflavin (LF, R = methyl at N10), riboflavin (RF, R = ribityl at N10, vitamin B_2), and flavin mononucleotide (FMN, R = ribophosphate at N10). Because the tricyclic aromatic flavin chromophore can absorb in a wide spectral range of the optical part of the electromagnetic spectrum, nature utilizes flavins and flavoproteins for many photochemical phenomena, redox reactions, and biocatalytic processes.[1–5] Examples include the repair of DNA, blue light receptors (BLUF), light-oxygen-voltage (LOV) sensing, the respiratory chain, and the catalytic oxidation of glucose by GOx enzymes. The importance of flavins was appreciated by (i) the Nobel prize in chemistry in 1937 awarded to Karrer for his pioneering synthesis and characterization of flavins, and (ii) the Nobel prize in chemistry in 2015 awarded to

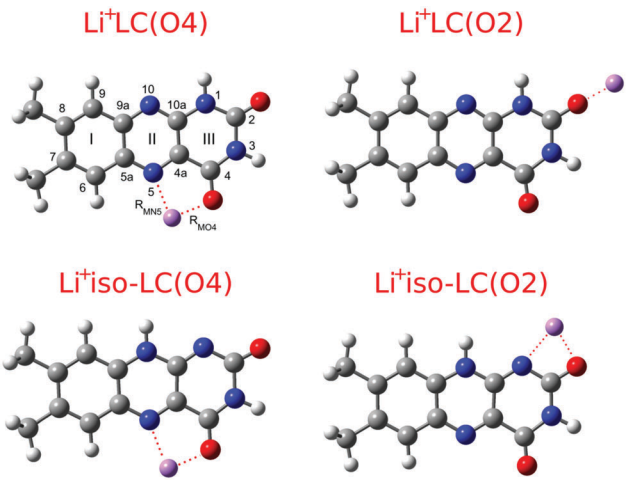

Fig. 1 Lowest-energy structural isomers of Li^+LC (LC = $C_{12}N_4O_2H_{10}$, O atoms are red, N atoms are blue) calculated at the PBE0/cc-pVDZ level. Atomic and ring numbers according to IUPAC notation are indicated for Li^+LC(O4). The M–N5 (R_{MN5}) and M–O4 (R_{MO4}) bond distances are also indicated.

[a] *Institut für Optik und Atomare Physik, Technische Universität Berlin, Hardenbergstr. 36, Berlin D-10623, Germany. E-mail: dopfer@physik.tu-berlin.de; Fax: +49 30 314 23018*

[b] *Laboratory for Chemistry and Life Science, Institute of Innovative Research, Tokyo Institute of Technology, 4259, Nagatsuta-cho, Midori-ku, Yokohama, Japan*

† Electronic supplementary information (ESI) available. See DOI: 10.1039/c8cp03950j

Lindahl, Modrich, and Sancar for unraveling the mechanism of DNA repair involving the enzyme photolyase with its fully reduced flavin-adenine dinucleotide ($FADH^-$) chromophore. A variety of biochemical processes involving flavins are based on strong metal–flavin interactions.[6–15]

The optical absorption of flavins sensitively depends on the substituent (R), the protonation, metalation, and oxidation state, and the solvent environment. Therefore, the absorption spectrum is a valuable indicator for changes in the electronic structure of the flavin. To this end, the photochemical properties of flavins were extensively characterized in the condensed phase.[16–18] In contrast, spectroscopic studies of flavins and their aggregates isolated in the gas phase, which are required to separate the intrinsic structural, electronic, and chemical properties of the optically active flavin chromophore from the strong effects of the environment (*e.g.*, solvation, ions), have not been performed until recently. Apart from our contributions outlined below,[19–23] the few available studies from other groups include a fluorescence spectrum of LF embedded in He droplets,[24] the measurement of proton and electron affinities of LF by mass spectrometry,[25] and photo- and collision-induced fragmentation of protonated FMN.[26] Very recently, the optical absorption and emission spectra of the mono-anion of flavin adenine dinucleotide (FAD) have been reported in the 210–550 nm range, covering the first four excited singlet states (S_1–S_4).[27,28] However, the spectra recorded at room temperature exhibit rather broad and unstructured absorption and emission bands, which are similar to those in solution and do not provide any detailed structural or vibronic information.

A few years ago, we initiated a research program to systematically characterize the geometric and electronic structure of protonated and metalated flavins in the gas phase in the electronic ground (S_0) and first excited singlet states (S_1).[19–23] In this approach, the flavin ions are generated in electrospray ionization sources attached to tandem mass spectrometers. Their geometric and vibrational structures in the S_0 state are initially probed by infrared multiple photon dissociation (IRMPD) spectroscopy of mass-selected ions performed at room temperature in a Fourier-transform ion cyclotron resonance mass spectrometer coupled to an IR free electron laser.[19–21] In a second step, the vibronic structure in the S_1 state is measured by visible photodissociation (VISPD) of mass-selected ions in a tandem mass spectrometer (quadrupole/time-of-flight) coupled to a recently commissioned cryogenic ion trap (T = 4–300 K), using dye and optical parametric oscillator (OPO) lasers.[22,23] Significantly, both the IRMPD and VISPD spectra display vibrational resolution and thus provide for the first time very detailed information about (i) the preferred protonation and metalation sites and (ii) the effects of protonation and metalation on the geometric and electronic structure of isolated flavins. This information is extracted by comparison of the experimental spectra with results from density functional theory (DFT) calculations.

Herein, we present the vibronic VISPD spectra of the S_1 state of cryogenic M^+LC complexes with alkali ions (M = Li–Cs). The previous IRMPD studies indicate two major binding sites of M^+ to LC.[20] In the most stable O4 isomer, the M^+ ion binds to the lone pairs of O4 and N5 in a O4–M^+–N5 chelate type bonding, while in the less stable O2 isomer M^+ forms a linear C–O2–M^+ bond (Fig. 1). The analysis of the IRMPD spectra in the informative C=O stretch range reveals that the O4 isomer is clearly present for all alkali ions, while the O2 isomer is positively identified only for M = K–Cs. No evidence was obtained for the presence of M^+iso-LC complexes. For alkali ions, the M^+–LC interaction is mainly electrostatic in nature, and the bond strength scales with the inverse ionic radius of M^+.[20] The interaction with coinage metals ions (M = Cu and Ag) is stronger because of additional covalent contributions to the M^+–LC bond involving transition metals. Interestingly, the only structure found for protonated LC (H^+LC) is the N5 isomer, in which the proton forms a covalent N5–H bond.[19] The proton is too small to benefit from the interaction with the lone pairs of both N5 and O4. Thus, the resulting two deep H^+LC(N5) and H^+LC(O4) minima are well separated by a large barrier, and only H^+LC(N5) is detected in the IRMPD experiment. This isomer assignment was subsequently confirmed by the analysis of the optical spectrum of the S_1 state of H^+LC.[22,23]

As outlined above, the optical absorption properties of isolated flavins are relevant for many photochemical processes and are essentially unexplored. The electronic structure is dominated by ππ* excitation of the aromatic π electrons and nπ* excitation of the in-plane lone pair electrons of the various O and N atoms of the heterocyclic chromophore.[3,16,29–31] The case of LC as the smallest flavin is particularly interesting.[30] The lowest excited singlet state (S_1) was predicted to be a dark nπ* state. Consequently, only the nearby optically bright ππ* transitions were observed in the liquid phase.[16] No gas phase spectrum of isolated LC has been reported so far. The analysis of our recent vibronic VISPD spectrum of cryogenic H^+LC(N5) ions recorded at $T \sim 25$ K reveals important effects of N5-protonation on the electronic structure and molecular orbitals of LC.[23] In particular, a large red shift of the optically bright $S_1 \leftarrow S_0$ (ππ*) transition upon protonation ($\Delta S_1 \sim -6000$ cm^{-1}) is observed, in agreement with the quantum chemical predictions. Significantly, N5-protonation of LC switches the energetic order of the lowest nπ* (dark) and ππ* (bright) states from S_1/S_2 to S_2/S_1.[23] Herein, we extend this work for H^+LC to M^+LC complexes with the alkali ions M = Li–Cs, using the same experimental and computational strategy, to further explore the effects of a metal cation on the optical absorption of this chromophore as a function of the interaction strength and the binding site. Significantly, these VISPD spectra are the first optical spectra of any isolated metal–flavin complex. Thus, the results provide a first impression of the $M^+\cdots$flavin interaction and its dependence on electronic excitation.

2. Experimental and computational details

VISPD spectra of cryogenic M^+LC ions are recorded in the BerlinTrap tandem mass spectrometer described elsewhere.[22] Briefly, the BerlinTrap setup includes (i) an electrospray ionization

(ESI) source to produce the ions, (ii) a mini-quadrupole to accumulate the ions, (iii) a quadrupole mass filter to select the ions under study, (iv) a cryogenic 22-pole ion trap to store and cool the ions by means of He buffer gas, and (v) a reflectron time-of-flight mass spectrometer (ReTOF-MS) to detect the parent and fragment ions. M^+LC ions are generated in the ESI source by spraying a solution containing LC at a rate of 2 mL h^{-1}. For the production of M^+LC, 2 mg LC are added to 19 mL methanol and 1 mL water (to increase salt solubility), with 0.14–0.10 mmol of alkali salt (LiCl–CsCl, Sigma Aldrich, >99.9% purity), giving average mole ratios of about 1 : 12 of neutral LC to metal salt (to optimize the yield of M^+LC ions). The M^+LC ions generated are mass selected and guided to the cryogenic 22-pole trap mounted on a coldhead, where they are cooled down to 25 K using pulsed He buffer gas and stored for 90 ms. After extraction from the trap, the cold M^+LC ions are irradiated at the extraction region of the orthogonal ReTOF-MS, and both fragment and parent ions are simultaneously detected by a microchannel plate. For all M^+LC parent ions, M^+ is the only fragment ion observed upon VISPD (see Fig. 2 for M = Cs). Laser radiation is provided by a commercial OPO laser (Continuum, Panther EX-OPO) pumped by the third harmonic of a Nd:YAG laser (Continuum, Powerlite DLS 9010). Typical OPO laser intensities are 3–5 mJ per pulse at an area of around 2 cm^2. The laser wavelength (bandwidth ~2 cm^{-1}) is tuned using 0.02 nm steps and calibrated with a wavemeter. In addition, a dye laser (Radiant Dyes, Narrowscan) pumped by the third harmonic of a Nd:YAG laser (Innolas, Spitlight 1000) is used for the Na–Cs experiments to improve the spectral resolution compared to the corresponding spectra recorded with the OPO laser. Coumarin 120 and Stilbene dissolved in ethanol are employed as dye solutions for recording the spectra of M^+LC with M = Na and K–Cs, respectively. Pulse energies of 5–9 mJ at a bandwidth of 0.06 cm^{-1} are obtained with this laser. The frequency of the dye laser is also calibrated with the wavemeter. The mass discriminated ion signals registered at the microchannel plate are converted into VISPD action spectra by linear normalization of the integrated M^+ fragment ion signal by both the M^+LC parent ion signal and the laser intensity measured simultaneously with the photodissociation mass spectra. To cover the respective $S_1 \leftarrow S_0$ transitions of M^+LC, their VISPD spectra are recorded in the 21 300–24 700 cm^{-1} spectral range.

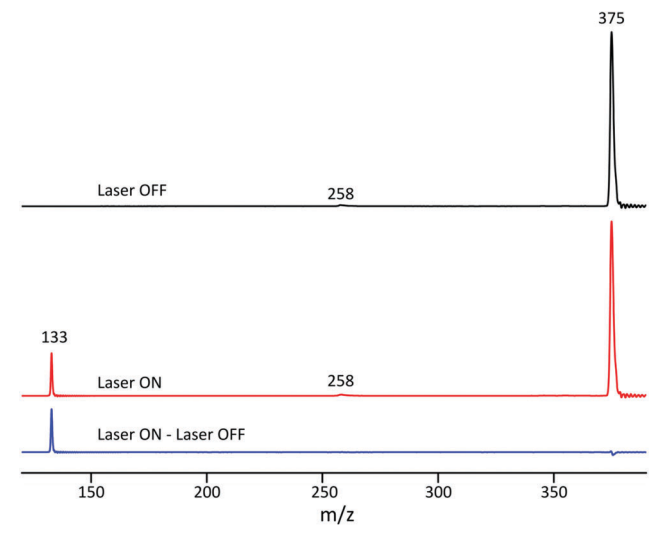

Fig. 2 Photodissociation mass spectra of Cs^+LC (*m*/*z* 375). Laser ON, laser OFF, and difference mass spectra with the laser frequency tuned resonantly to the $S_1 \leftarrow S_0$ band origin at 23 571 cm^{-1}. The only laser-induced fragment ion is Cs^+ (*m*/*z* 133). The laser-induced loss of LC is observed for all M^+LC with alkali ions. A low-intensity fragment ion not sensitive to laser action is observed at *m*/*z* 258 and arises from metastable decay or collision-induced dissociation.

DFT calculations at the PBE0/cc-pVDZ level are carried out for optimizing the electronic ground states (S_0) of LC, iso-LC, and their M^+LC and M^+iso-LC isomers using GAUSSIAN09.[32] Vertical excitation energies of the ground state minima are calculated with the time-dependent DFT approach. Subsequently, geometries of the first excited electronic states (S_1–S_3) are optimized at the same computational level using the corresponding ground state structures as starting point. The computationally economic PBE0 functional is chosen because it reproduces the vibronic $S_1 \leftarrow S_0$ spectrum of the related H^+LC ion well.[23] This functional also yields similar results for the S_0 ground state as the B3LYP functional employed previously for the analysis of the IR spectra of flavin ions[19–21] but yields much better predictions for the excited state spectra.[23] Harmonic vibrational analysis ensures the identification of minima on the potential energy surface. The natural transition orbitals method[33] is employed to determine the orbitals involved in the lowest electronic excitations. Calculated metal ion binding energies (D_0) and relative energies (ΔE_0) are corrected for harmonic zero-point vibrational energies. Vibronic spectra are simulated for T = 0 K utilizing harmonic (unscaled) frequencies by means of multi-dimensional Franck–Condon (FC) simulations as implemented in PGOPHER.[34] These stick spectra are convoluted with a Lorentzian line profile using a FWHM of 6 cm^{-1} to enable convenient comparison with the measured VISPD spectra. The atomic charge distribution is evaluated using the natural bond orbital analysis.[35]

3. Results and discussion

The VISPD spectra of the $S_1 \leftarrow S_0$ transition of all M^+LC ions considered (M = Li–Cs) are recorded in the LC loss channel, which is the only fragmentation channel observed upon photodissociation. As an example, the laser-on and laser-off mass spectra of Cs^+LC (*m*/*z* 375) obtained with the laser frequency tuned resonantly to its $S_1 \leftarrow S_0$ band origin at 23 571 cm^{-1} are shown in Fig. 2. The only laser-induced fragment ion observed is Cs^+ (*m*/*z* 133). The other minor fragment ion at *m*/*z* 258 is not affected by laser action and is thus concluded to result from metastable decay and/or collision-induced dissociation. The VISPD spectra of all M^+LC ions recorded in the vicinity of the S_1 origin are compared in Fig. 3 to that of H^+LC.[23] These spectra are referenced to the S_1 origins, and spectra at the absolute wavenumber scale are available in Fig. S1 in ESI† to show the complete covered range. The 22-pole trap temperature is kept at

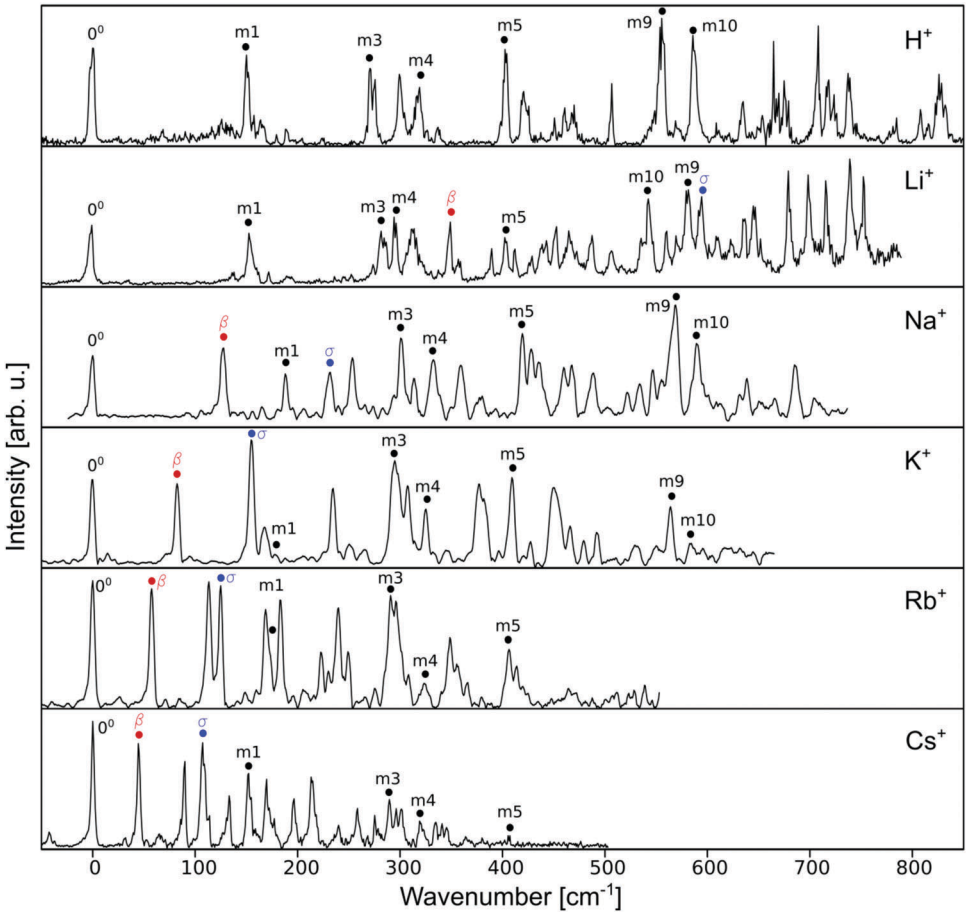

Fig. 3 Experimental VISPD spectra of the $S_1 \leftarrow S_0$ transition of M^+LC (M = H, Li–Cs) plotted as a function of S_1 internal energy. The spectra of H^+LC and Li^+LC are recorded with the OPO laser, while the dye laser is used for the spectra of M^+LC with M = Na–Cs. The S_1 origin energies (0^0) are 19 962 (H), 21 911 (Li), 22 786 (Na), 23 315 (K), 23 465 (Rb), and 23 571 cm^{-1} (Cs). Spectra at the absolute wavenumber scale are available in Fig. S1 in ESI.† Positions and assignments of vibronic transitions are listed in Table S1 in ESI.† Intramolecular LC modes are denoted as m1–m10, while β and σ are intermolecular in-plane $M^+\cdots$LC bend and stretch modes. The spectrum of H^+LC is reproduced from ref. 23.

25 K for all measurements (except for Li^+LC, for which the trap is held at 6 K) to maximize the trapped ion and VISPD signals. This temperature is low enough to nearly completely suppress the appearance of hot bands for all M^+LC ions except for Cs^+LC. Cs^+LC has the lowest vibrational frequencies, because it has the weakest $M^+\cdots$LC bond and the highest mass. VISPD spectra of Cs^+LC recorded for various ion trap temperatures (T = 25, 50, 100 K) illustrate the drastic effect of cooling the rotational and vibrational temperature of the ions on the widths of the vibronic transitions and the intensity of hot bands (Fig. S2 in ESI†). A FC analysis of the relative intensity of the 53_1^0 hot band originating from the lowest frequency mode in S_0 (β = 42 cm^{-1}) yields a vibrational temperature of 29 ± 3 K for a nominal trap temperature measured as 25 ± 1 K. Similar ion temperatures of 33 ± 3 and 31 ± 3 K are obtained for K^+LC and Rb^+LC from the analysis of the hot band intensities. For M^+LC with M = Li and Na no hot bands are detected. The widths of the peaks in the M^+LC spectra with M = Na–Cs recorded with the dye laser (bandwidth ~0.06 cm^{-1}) are ~3–4.5 cm^{-1} at T = 25 K and arise mostly from unresolved rotational structure (and possibly from a finite lifetime). The Li^+LC spectrum exhibits slightly larger widths (~5 cm^{-1} for the S_1 origin), because it is measured with the OPO laser (bandwidth ~2 cm^{-1}). The S_1 origin of all M^+LC ions is accompanied by rich vibronic structure, indicating a large geometry change upon electronic excitation. The S_1 origin energies of 21 911 (Li), 22 786 (Na), 23 315 (K), 23 465 (Rb), and 23 571 cm^{-1} (Cs) increase substantially with increasing size of the alkali ion. Unfortunately, no experimental spectrum is available for isolated LC. The maximum of its first absorption band in solution (assigned to the lowest ππ* state, S_2) lies in the 379–385 nm range (~26 000 cm^{-1}) depending on the solvent.[16] Assuming this value as an experimental reference energy for the lowest ππ* state of isolated LC, the large derived S_1 red shifts of −2429 (Cs) and −4089 cm^{-1} (Li) for M^+LC illustrate that metalation of the aromatic chromophore significantly changes both its geometric and electronic structure. On the other hand, the S_1 red shifts of M^+LC are smaller than that of H^+LC (~−6000 cm^{-1} for the observed N5-protonated isomer), indicating that the effects of alkali metal complexation are less pronounced than that of protonation.[23]

Quantum chemical calculations are used to derive the isomer and vibronic assignments of the measured VISPD spectra.

The M^+ cation can bind to the various available nucleophilic sites of LC and iso-LC (Fig. 1), including the lone pairs of the O atoms of the two CO groups (denoted O2 and O4), the lone pairs of the two heterocyclic N atoms (N5 and N10 for LC, N1 and N5 for iso-LC), and π-stacking to the three aromatic rings (I–III).[20] However, only isomers with M^+ attached to the CO groups of LC are found experimentally by IRMPD spectroscopy.[20] Consequently, only these will be considered in detail here. Although LC is predicted to be $\Delta E_0 = 55$ kJ mol^{-1} more stable than iso-LC, M^+iso-LC complexes may still be present in solution and in the ESI spray because of enhanced solvent stabilization. In fact, our previous IRMPD experiments on M^+LC reveal the presence of isomers with relative energies as high as 40 kJ mol^{-1} in the ESI source.[20] The binding and relative energies D_0 and ΔE_0 of all considered M^+LC isomers calculated at the PBE0 level agree well with those at the B3LYP level.[20] The M^+LC(O4) isomer, in which M^+ binds in a chelate to the lone pairs of both O4 and N5, is the global minimum for all alkali ions,[20] with D_0 ranging from 296 kJ mol^{-1} for Li^+ down to 140 kJ mol^{-1} for Cs^+. The M^+LC(O2) isomers, in which M^+ binds in a linear fashion to O2, are systematically less stable local minima, whereby the energy gap to the O4 minimum decreases from 73 (Li) to 34 kJ mol^{-1} (Cs). The geometric and vibrational properties of the O4 and O2 isomers of M^+LC in the S_0 ground electronic state are discussed in detail elsewhere.[20] In general, the $M^+\cdots$LC bond is mostly electrostatic in nature. Hence, the bond strength, and several other structural and spectroscopic parameters, show a monotonic dependence on the inverse ionic radius of M^+ ($1/R_M$).[20,21,36] While the most stable M^+LC(O4) isomer is identified in the IRMPD spectra of all alkali ions, the M^+LC(O2) local minimum is positively identified only for M = K–Cs.[20] The O2 isomer of M^+iso-LC (O2/N1 chelate) is slightly more stable (by 2–12 kJ mol^{-1}) than the corresponding O4 isomer (O4/N5 chelate). Both M^+iso-LC isomers are less stable than the M^+LC(O4) global minimum by around 45–60 kJ mol^{-1}. This energy difference is mainly coming from the difference in stability of LC and iso-LC.

To identify the M^+LC isomers observed in the VISPD spectra, both the positions of the adiabatic $S_1 \leftarrow S_0$ origin transitions and the vibronic spectra simulated within the FC approximation are considered next. In Fig. 4 the experimental S_1 origins extracted from the VISPD spectra are compared with the adiabatic S_1 origins calculated for all considered isomers and plotted *versus* the inverse ionic radii $(1/R_M)$[20,36] of M^+. A monotonic dependence of the metalation-induced S_1 shift on $1/R_M$ is expected, because the $M^+\cdots$LC bonding is mostly electrostatic for all alkali ions.[20] The data points for the O4 and N5 isomers of H^+LC discussed elsewhere[23] are also included for completeness. The experimental VISPD spectra of M^+LC are compared in Fig. 5 to the simulated $S_1 \leftarrow S_0$ vibronic spectra as a function of the S_1 internal energy. The computed spectra have to be shifted by a constant amount to match the calculated and experimental S_1 origins, $\Delta\nu = S_1^{exp} - S_1^{calc}$. All values for S_1^{exp}, S_1^{calc}, and $\Delta\nu$ are listed in Table 2. The spectra of the calculated isomers are ordered from top to bottom according to their relative energy (Table 1).

From Fig. 4, it is evident that the adiabatic S_1 energies calculated for the M^+LC(O4) isomer closely reproduce the trend

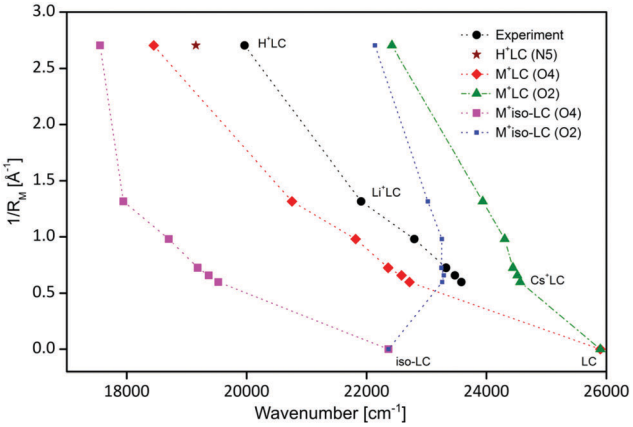

Fig. 4 Measured adiabatic $S_1 \leftarrow S_0$ (ππ*) transition energies of M^+LC (black dots) compared to values calculated for the various M^+LC and M^+iso-LC conformers (M = H, Li–Cs) (colored symbols) *versus* the inverse radius of the cation.[20,36] The values for the O4 (M = Li–Cs) and N5 (M = H)[23] conformers reproduce the experimental trend best except for a nearly constant shift ranging from +1154 (Li) to +854 cm^{-1} (Cs) and down to +809 cm^{-1} for the protonated species (Table 2). The data point calculated for LC corresponds to the S_2 state, because S_2 is the lowest ππ* state for LC.

of the experimental data, with a small and roughly constant deviation of $\Delta\nu = 1004 \pm 150$ cm^{-1} (~5%, ~0.1 eV). The deviation $\Delta\nu$ becomes slightly smaller with decreasing interaction ($\Delta\nu$ = 1154, 969, 955, 881, and 854 cm^{-1} for Li to Cs). In addition, extrapolation to zero interaction ($R_M \rightarrow \infty$) converges smoothly to the value computed for the corresponding S_2 state of LC (*i.e.*, the lowest bright ππ* state). (Here, we note that the S_1 state of LC is in fact predicted to be a dark nπ* state at 24 826 cm^{-1}, which however is calculated to be very close to the optically bright ππ* state (S_2), with an adiabatic energy difference of 1073 cm^{-1}). The energies of the S_1 origins computed for the M^+LC(O2) isomers exhibit a largely different dependence as a function of $1/R_M$. In addition, they are significantly larger than the experimental values ($-\Delta\nu$ = 2026, 1517, 1126, 1050, and 992 cm^{-1} for Li to Cs). For both reasons, we can exclude the O2 isomers. The S_1 origins of M^+iso-LC(O4) are systematically lower than the measured values by around 4000 cm^{-1} ($\Delta\nu$ = 3966, 4085, 4131, 4097, 4043 cm^{-1} for Li to Cs), and this large difference of ~0.5 eV allows us to exclude also this isomer as carrier of the measured VISPD spectra. Finally, although the S_1 origins of M^+iso-LC(O2) are closer to the observed ones ($\Delta\nu$ = −1111, −470, 67, 176, 309 cm^{-1} for Li to Cs), the largely varying deviations indicate that this isomer is also not responsible for the observed spectra. The large differences in the computed S_1 origins of M^+LC(O4) and M^+LC(O2) illustrate that the optical absorption properties and thus the photochemical behaviour of flavins can indeed be drastically manipulated by metal complexation, because they strongly depend on both the type of metal ion and the metalation site.

The comparison of the computed vibronic spectra of the various isomers with the measured VISPD spectra in Fig. 5 confirms the assignment to the most stable M^+LC(O4) isomer derived from the analysis of the S_1 origins. Clearly, all intense vibrational features are well reproduced in position and relative

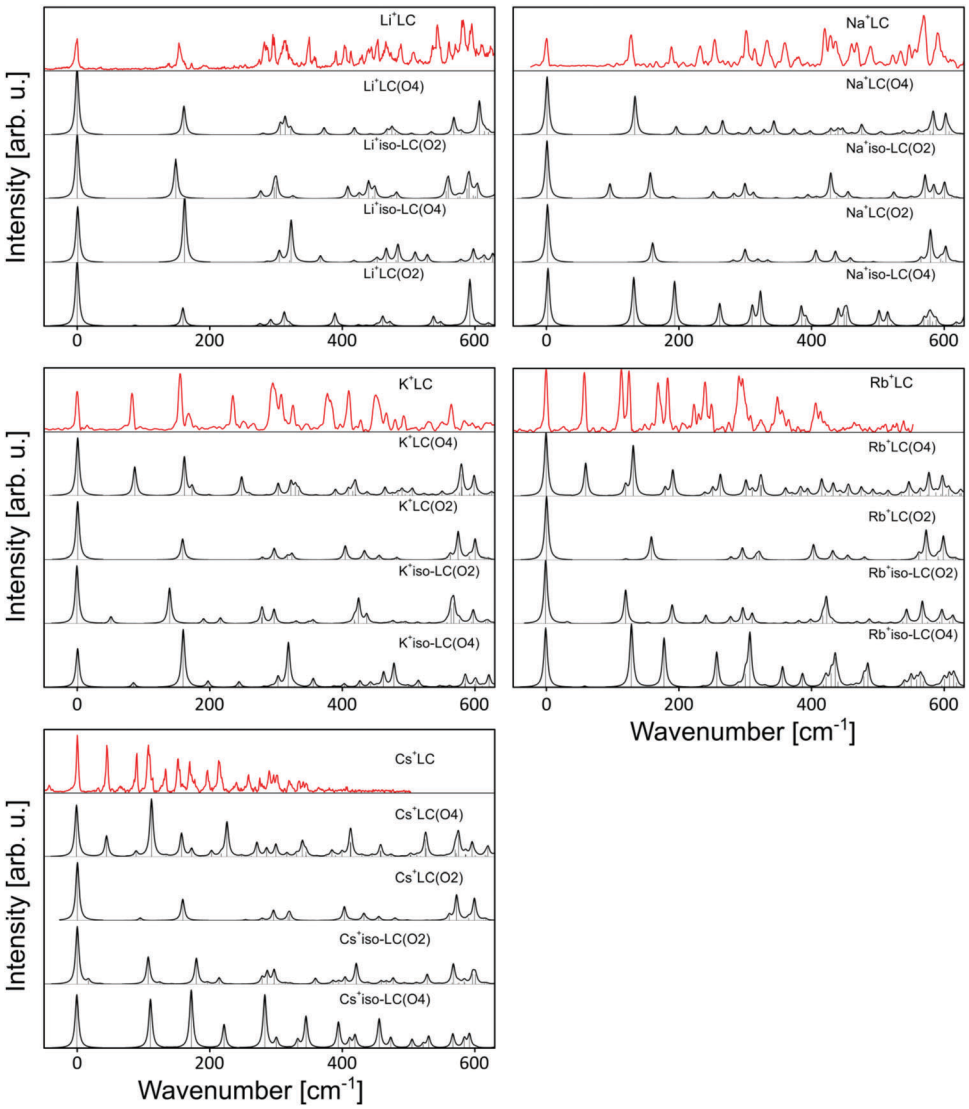

Fig. 5 Comparison between experimental VISPD spectra recorded for M^+LC (M = Li–Cs) as a function of S_1 internal energy (Fig. 3) compared to Franck–Condon simulations for the isomers shown in Fig. 1 using a convolution width of 6 cm^{-1}. Isomers are ordered from top to bottom according to their relative energy (Table 1).

intensity only for this isomer for all metal ions. For example, for M = K–Cs only the $M^+LC(O4)$ spectrum can reproduce the first vibronic band. On the other hand, the first vibronic band predicted for M^+iso-LC(O2) with M = Na–Cs is not detected in the experiment. Hence, from the overall analysis of the relative energies, binding energies, S_1 energies, and vibronic spectra, we clearly favor an assignment of the VISPD spectra to the most stable $M^+LC(O4)$ isomer, which is also the dominant isomer identified by IRMPD spectroscopy.[20] The presence of other isomers in the VISPD spectra in the same spectral range is unlikely, considering the large differences in their predicted S_1 origins (Fig. 4 and Table 2).

After the identification of the $M^+LC(O4)$ isomer as the carrier of the observed VISPD spectra for all alkali metals, we focus in Fig. 6 on the detailed assignment of the vibronic transitions. Numerical values for the positions of all intense experimental bands and their vibronic assignments are given in Table S1 in ESI.† Complete lists of all vibrational frequencies calculated for the S_0 and S_1 states of $M^+LC(O4)$ are available in Table S2 in ESI.† The numbering of the vibrational modes follows the Mulliken notation. The $M^+LC(O4)$ structures with their planar aromatic rings have C_s symmetry, and the $S_1 \leftarrow S_0$ transition has $\pi\pi^*$ character. Consequently, according to the FC principle, all vibronic transitions originating from the ground vibrational state in the S_0 electronic ground state terminate in S_1 vibrational states with a' symmetry, *i.e.* only in-plane modes (a') are observed and assigned. The maximum deviations between the experimental and calculated harmonic vibrational frequencies are less than 20 cm^{-1}, with mean deviations of around 5–10 cm^{-1} for M = Li–Cs. These differences are small considering the experimental peak width ($\sim$5 cm^{-1}) and the harmonic approximation employed for the FC analysis. Most of the vibronic transitions

Table 1 Binding energies (D_0) and relative energies (ΔE_0) in kJ mol^{-1} calculated at the PBE0/cc-pVDZ level compared to corresponding values determined at the B3LYP/cc-pVDZ level[a]

	PBE0/cc-pVDZ		B3LYP/cc-pVDZ			PBE0/cc-pVDZ		B3LYP/cc-pVDZ	
Isomer	D_0	ΔE_0	D_0	ΔE_0	Isomer	D_0	ΔE_0	D_0	ΔE_0
LC		0			K^+LC(O4)	173.6	0	177.4	0
iso-LC		54.9			K^+LC(O2)	131.8	41.8	137.4	40.0
Li^+LC(O4)	296.0	0	304.0	0	K^+iso-LC(O2)	182.4	46.1		
Li^+iso-LC(O2)	294.4	56.5			K^+iso-LC(O4)	170.9	57.6		
Li^+iso-LC(O4)	292.0	58.9			Rb^+LC(O4)	155.4	0	156.6	0
Li^+LC(O2)	222.7	73.3	232.5	71.5	Rb^+LC(O2)	116.8	38.6	120.2	36.4
Na^+LC(O4)	217.6	0	223.6	0	Rb^+iso-LC(O2)	164.8	45.5		
Na^+iso-LC(O2)	221.6	50.9			Rb^+iso-LC(O4)	153.1	57.3		
Na^+LC(O2)	161.1	56.4	168.0	55.6	Cs^+LC(O4)	140.3	0	140.3	0
Na^+iso-LC(O4)	213.5	59.0			Cs^+LC(O2)	106.3	34.0	108.8	31.5
					Cs^+iso-LC(O2)	150.8	44.4		
					Cs^+iso-LC(O4)	138.7	56.5		

[a] B3LYP values are from ref. 20.

Table 2 Experimental and predicted adiabatic S_1 energies of LC and various isomers of M^+LC and M^+iso-LC calculated at the PBE0/cc-pVDZ level, along with the shifts from the experimental S_1 origin (in cm^{-1})

Isomer	$S_1 \leftarrow S_0$	$\Delta\nu$	Isomer	$S_1 \leftarrow S_0$	$\Delta\nu$
LC(exp)	~26 000 (S_2)[a]		K^+LC(exp)	23 315	0
LC	25 899 (S_2)[b]		K^+LC(O4)	22 360	955
iso-LC	22 366		K^+LC(O2)	24 441	−1126
H^+LC(exp)[c]	19 962	0	K^+iso-LC(O2)	23 248	67
H^+LC(N5)[c]	19 153	809	K^+iso-LC(O4)	19 184	4131
H^+LC(O4)[c]	18 451	1511	Rb^+LC(exp)	23 465	0
Li^+LC(exp)	21 911	0	Rb^+LC(O4)	22 584	881
Li^+LC(O4)	20 757	1154	Rb^+LC(O2)	24 515	−1050
Li^+iso-LC(O2)	23 022	−1111	Rb^+iso-LC(O2)	23 289	176
Li^+iso-LC(O4)	17 945	3966	Rb^+iso-LC(O4)	19 368	4097
Li^+LC(O2)	23 937	−2026	Cs^+LC(exp)	23 571	0
Na^+LC(exp)	22 786	0	Cs^+LC(O4)	22 717	854
Na^+LC(O4)	21 817	969	Cs^+LC(O2)	24 563	−992
Na^+iso-LC(O2)	23 256	−470	Cs^+iso-LC(O2)	23 262	309
Na^+LC(O2)	24 303	−1517	Cs^+iso-LC(O4)	19 528	4043
Na^+iso-LC(O4)	18 701	4085			

[a] Vertical value from experiments in solution for the S_2 ($\pi\pi^*$) state (exact value depends on solvent).[16] [b] This value corresponds to the adiabatic energy of the optically bright $\pi\pi^*$ (S_2) state. For LC, this state is higher than the optically dark $n\pi^*$ (S_1) state at 24 826 cm^{-1}. [c] From ref. 23.

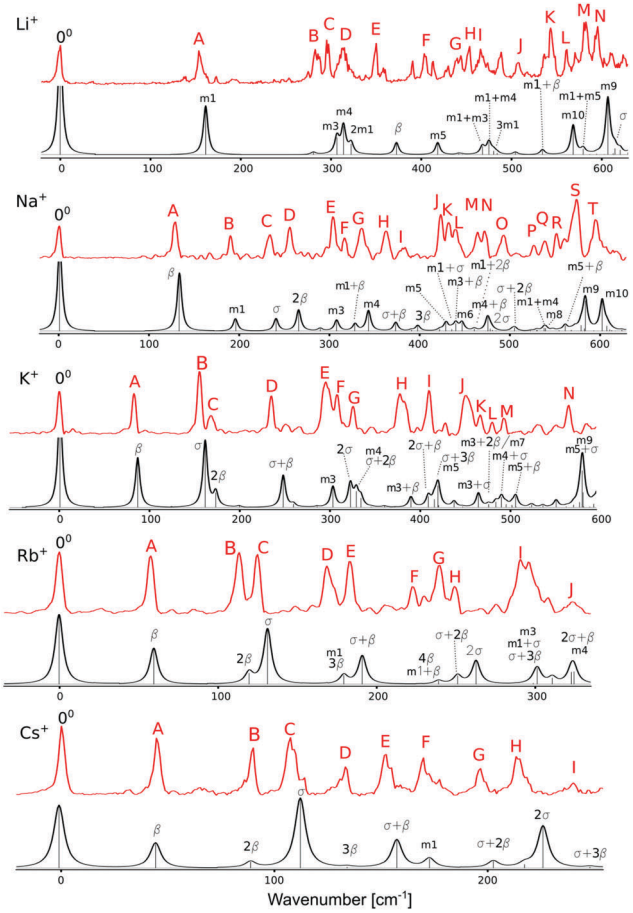

Fig. 6 Experimental VISPD spectra of M^+LC (M = Li–Cs) as a function of S_1 internal energy (Fig. 3) (top) compared with the Franck–Condon simulation of the identified M^+LC(O4) conformer (bottom) along with vibrational assignments (Table S1 in ESI†).

are fundamentals of the lowest frequency a' modes (42^1–53^1 for Li–Cs), and all other assigned modes are overtones and combination bands of these in-plane modes. At this point, we note that there is weak vibronic structure in the VISPD spectra which cannot be reproduced by the FC simulations at T = 0 K. This additional signal is most pronounced in the Li^+LC spectrum in the 100–300 cm^{-1} range above the S_1 origin. Similar signal was also observed in the H^+LC spectrum. The relative intensity of this signal strongly depends on the experimental conditions. According to the calculations, this signal cannot be ascribed to S_1 vibronic bands of other M^+LC isomers and also not to hot bands of M^+LC(O4). Alternative options including (i) vibronic bands of a higher electronic state of the M^+LC(O4) isomer and (ii) vibronic coupling of the bright S_1 state of M^+LC(O4) with another, possibly dark state, can also be excluded. Thus, we tentatively assign this signal to S_1 spectra of tagged M^+LC(O4)–L_n clusters with weakly bonded ligands L (*e.g.*, L = He and N_2) formed in the 22-pole trap. Such clusters are formed in various abundances depending on the experimental conditions, as observed in the mass spectra (not shown here). Their formation is only significant for Li^+LC (and H^+LC) because of the large binding energies of L to the small M^+ (H^+) ion.

Table 3 Frequencies (cm^{-1}) of relevant low-energy vibrations of M^+LC(O4) and LC in the S_0 and S_1 states calculated at the PBE0/cc-pVDZ level compared to available experimental S_1 frequencies. A complete set of calculated frequencies is given in Table S2 in ESI. For comparison, values are also given for H^+LC(N5) and LC

	Li			Na			K			Rb			Cs			H			LC	
Mode	S_0	S_1	exp	S_0	S_1	exp	S_0	S_1	exp	S_0	S_1	exp	S_0	S_1	exp	S_0	S_1	exp	S_0	S_1
β	354	373	350	123	132	128	79	86	83	55	60	57	42	45	45	1151	1143			
σ	598	615	595	233	240	232	156	161	155	122	132	125	104	114	108	3455	3555			
m1	159	161	157	187	195	189	190	199		176	180	182	171	174	170	153	153	154	159	158
m2	294	280		303	289		299	285		297	283		296	283		305	289	278	289	278
m3	310	306	288	314	307	301	309	303	295	308	301	293	308	301		283	274	274	303	296
m4	325	314	299	344	342	333	336	328	325	334	325	323	333	322		330	315	321	328	314
m5	414	418	403	428	428	420	419	419	410	416	416		414	413		413	412	406	406	404
m6	446	446		445	445	436	440	437		440	435		439	434		432	431		436	430
m7	481	480		479	477		478	476	466	478	475		478	475		474	472		475	471
m8	496	505		541	538	534	539	535		538	534		537	533		525	520	509	529	522
m9	623	607	596	616	582	569	613	579	565	612	577		612	576		573	570	558	607	564
m10	568	569	548	586	601	590	585	598		584	598		584	597		609	599	590	581	592

In a next step, we discuss the relevant low-frequency in-plane normal modes of the M^+LC(O4) isomer and compare their frequencies as a function of M^+. They are listed in Table 3 with an M^+-independent notation, and graphical representations are shown in Fig. S3 in ESI.† The two in-plane intermolecular modes of the metal ion are the $M^+\cdots$LC stretch (σ) and in-plane bend (β). Their frequencies change drastically with M^+, because both the reduced mass and the force constants change according to the strongly varying binding energy and angular anisotropy of the $M^+\cdots$LC potential. For example, β = 373–45 cm^{-1} and σ = 615–114 cm^{-1} are computed for M^+LC(O4) with Li–Cs in the S_1 state, as a result of the strongly decreasing interaction and increasing mass with increasing size of the metal ion. On the other hand, the frequencies of the skeleton vibrations of LC do not change much with M^+ (as long as they do not strongly couple with the intermolecular metal modes). As a result, the frequency order of the metal and LC modes changes with M^+, and we introduce an additional to describe the normal modes of $M^+\cdots$LC, which is independent of M^+ (m1, m2, m3,... for the lowest frequency a' modes, Fig. S3 in ESI†). In addition, these M^+LC modes do not differ much from those of LC and H^+LC, because both protonation and metalation have not a large impact on these. Briefly, mode m1 with a calculated S_1 frequency of 161–199 cm^{-1} for Li–Cs involves in-plane bending of the outer aromatic rings I and III around the central ring II. Its larger frequency variation is caused by M^+-dependent mixing with σ and β. Mode m2 with 280–289 cm^{-1} is a scissoring motion of the methyl groups at C7 and C8. Mode m3 with 301–307 cm^{-1} is associated with a shear deformation of ring II along the N5–N10 axis, while mode m4 with 314–342 cm^{-1} is described by a uniform stretching of the three aromatic rings along the long molecular axis. Mode m5 at 413–428 cm^{-1} involves a compression of ring III combined with a scissoring motion of the two carbonyl groups. Modes m9 and m10 with 576–607 and 569–601 cm^{-1} are two complex delocalized deformation modes of all three rings.

The low-frequency part of the M^+LC(O4) spectra with M = Na–Cs is dominated by progressions and combinations of the intermolecular β and σ modes, indicative of substantial geometry changes of the $M^+\cdots$LC bond upon S_1 excitation. For example, all but one transition in the Cs^+LC(O4) spectrum can be assigned to $n\beta + m\sigma$ with $n \leq 3$ and $m \leq 2$. Bands A, B, and D are due to $n\beta$, bands C and H arise from $m\sigma$, and bands E, G, and I are combination bands of β and σ. The remaining band F is due to the intramolecular m1 mode of LC. The M^+LC(O4) spectra with M = Na–Rb exhibit similar intermolecular $n\beta + m\sigma$ transitions but contain more intramolecular LC bands (mainly m1–m5, m9, m10) toward higher frequency, because they are recorded in a more extended frequency range. Interestingly, the Li^+LC(O4) spectrum is dominated by intramolecular LC modes, and the β and σ modes with their high frequencies are less pronounced in the VISPD spectrum. In general, the computed metal frequencies β = 45, 60, 86, 132, and 373 cm^{-1} and σ = 114, 132, 161, 240, and 615 cm^{-1} (Cs–Li) agree very well with the measured ones (β = 45, 57, 83, 128, 350 cm^{-1}, σ = 108, 125, 155, 232, 595 cm^{-1}), indicating that the computational level describes the $M^+\cdots$LC interaction in the S_1 excited state to high accuracy. In addition, both in-plane metal frequencies are slightly larger in the S_1 state than in the S_0 state (β = 42, 55, 79, 123, 354 cm^{-1}, σ = 104, 122, 156, 233, 598 cm^{-1}), because the $M^+\cdots$LC interaction increases by S_1 excitation. This observation is consistent with the computed (and observed) S_1 red shifts upon metalation, because these correspond directly to the increase in the binding energy upon S_1 excitation ($\Delta D_0 = -\Delta S_1$). This strengthening of the $M^+\cdots$LC interaction amounts to ΔD_0 = 34.8, 24.4, 18.1, 16.3, and 12.9 kJ mol^{-1} for M^+LC(O4) with M = Li–Cs, which corresponds to 9–12%. Interestingly, the Li^+LC(O4) spectrum closely resembles that of H^+LC(N5), possibly because both Li^+ and H^+ bind very strongly to the LC chromophore so that electronic S_1 excitation does not affect much the geometry of the cation$\cdots$LC bond in these two ions.

In a next step, we consider in more detail the geometry changes of M^+LC(O4) induced by S_1 excitation, which are already indicated by the vibrational analysis. To this end, the geometry of the S_0 state and its change upon S_1 excitation are shown in Fig. 7 for Li^+LC(O4), while corresponding structures for M = Na–Cs are given in Fig. S4 in ESI.† Specifically, the structural changes of LC induced by metalation at the O4 position in the S_0 state are described in Fig. 7(top) (and Fig. S4(top) in ESI†), where relative

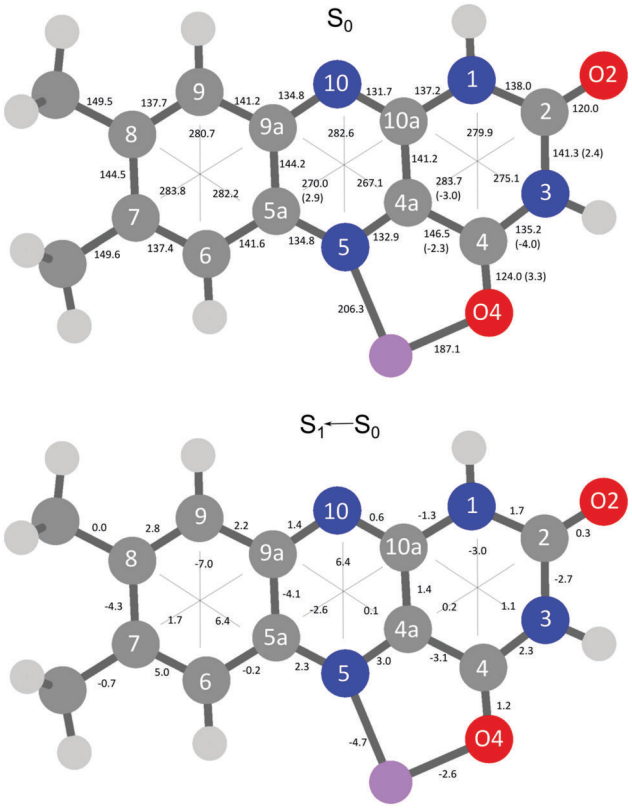

Fig. 7 (top) Geometry of the ground state (S_0) of Li^+LC (absolute values) and relative changes ≥2 pm compared to bare LC calculated at the PBE0/cc-pVDZ level. (bottom) Geometry changes of $Li^+LC(O4)$ upon S_1 excitation (distances relative to S_0). All values are given in pm. Positive values correspond to elongations; negative values indicate contractions upon S_1 excitation.

changes ≥2.0 pm with respect to neutral LC are given in parentheses. The metal ion binds slightly closer (and stronger) to O4 than to N5 (187.1 and 206.3 pm for Li) and the induced geometry changes are more important for ring III than for ring II, as discussed in detail previously.[20,23] The geometry change of $Li^+LC(O4)$ upon S_1 excitation of $Li^+LC(O4)$ visualized in Fig. 7(bottom) (and in Fig. S4(bottom) in ESI† for M = Na–Cs) is even more drastic than that induced by metalation. The consequences of S_1 excitation are substantial throughout the whole chromophore and particularly strong in rings I and II. The expansion of ring II along the N5–N10 axis (6.4 pm) is accompanied by a compression of the same ring along the C5a–C10a axis (−2.6 pm). Ring I is greatly contracted along the C9–C6 distance (−7.0 pm) and expanded along the C7–C9a (1.7 pm) and the C8–C5a (6.4 pm) directions. In contrast, only a smaller deformation is induced in ring III, with a contraction along the N1–C4 axis (−3.0 pm) and an elongation of the N3–C10a distance (1.1 pm). $S_1 \leftarrow S_0$ excitation also moderately affects the bond length of the C4O carbonyl group (1.2 pm). The structural changes of the LC moiety upon S_1 excitation of $M^+LC(O4)$ are relatively independent of M^+, because the orbitals involved in electronic ππ* excitation are localized on the LC chromophore and not on M^+ (Fig. 8). On the other hand, charge

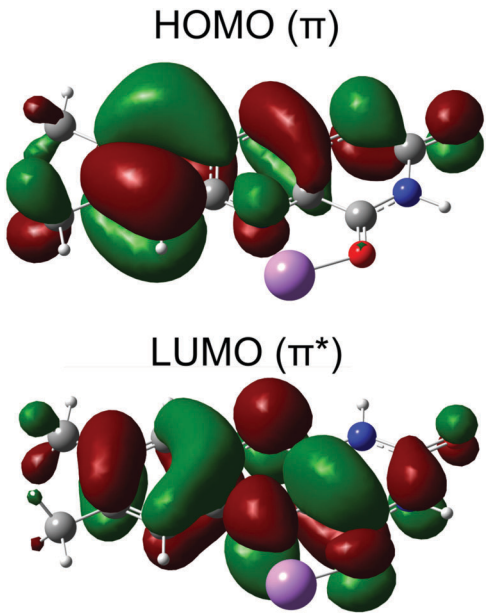

Fig. 8 Molecular orbitals involved in the $S_1 \leftarrow S_0$ transition (LUMO ← HOMO, ππ*) of $Li^+LC(O4)$ calculated at the PBE0/cc-pVDZ level.

reorganization involved in S_1 excitation of LC has a strong impact on the geometry of the $M^+\cdots LC$ bond in $M^+LC(O4)$, which depends somewhat on the interaction strength. As a result of the drastic increase in the $M^+\cdots LC$ interaction upon S_1 excitation (as indicated by the S_1 red shift), the intermolecular R_{MN5} and R_{MO4} distances contract for all metals. The contraction of the M–O4 bond is more pronounced for the heavier alkali ions (ΔR_{MO4} = −2.6, −3.4, −5.0, −5.7, −7.1 pm for Li–Cs). Interestingly, the M–N5 bond contraction is of similar magnitude but exhibits a nonmonotonic behaviour, with the smallest contraction obtained for K (ΔR_{MN5} = −4.7, −4.6, −4.4, −4.9, and −5.2 pm from Li to Cs), because also the N5–M–O4 chelate angle changes at the same time.[20] These large changes in the M–N5 and M–O4 bond lengths upon S_1 excitation are consistent with the long FC progressions of the $M^+\cdots LC$ intermolecular modes β and σ observed in the vibronic VISPD spectra of the $S_1 \leftarrow S_0$ transition.

The HOMO and LUMO orbitals involved in the $S_1 \leftarrow S_0$ transition of $M^+LC(O4)$ in Fig. 8 (shown for M = Li) illustrate its character as optically allowed ππ* excitation. Clearly, both orbitals are localized on the aromatic LC chromophore and have essentially no amplitude on M^+. Hence, the calculated oscillator strengths for S_1 excitation of $M^+LC(O4)$ are roughly constant ($f \times 10^3$ = 31, 40, 45, 49, 51 for M = Li–Cs). The same HOMO and LUMO orbitals have previously been identified to be responsible for the $S_1 \leftarrow S_0$ transition of $H^+LC(N5)$ by the same computational and spectroscopic approach ($f \times 10^3$ = 48).[23] As discussed earlier, the experimental S_1 red shift of $M^+LC(O4)$ observed for the lowest ππ* transition is in the 2429–4089 cm^{-1} range for Cs–Li, in good agreement with computed red shifts of 3182–5142 cm^{-1}. S_1 excitation of LC shifts electron density from ring I to ring II, in particular also to N5 and O4. For example, the atomic charges on O4 and N5 in LC are −0.565 and −0.386 *e* in S_0 and −0.595 and −0.477 *e* in the ππ* excited state (S_2), respectively

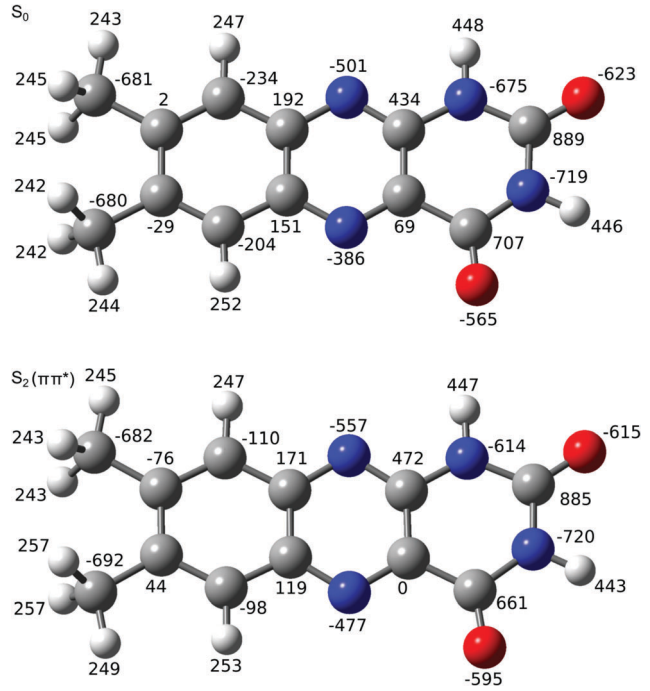

Fig. 9 Atomic charges (in units of 10^{-3} e) of LC in the S_0 and first ππ* excited state (S_2) evaluated at the PBE0/cc-pVDZ level using natural bond orbital analysis.

(Fig. 9 and Table 4). Hence, in the O4–M^+–N5 chelate, this charge transfer enhances the electrostatic interaction of LC with the nearby M^+ cation in the S_1 state of the M^+LC(O4) isomer, which results in the large S_1 red shift (Fig. 4). On the other hand, ππ* excitation has little impact on the partial charge of the O2 atom of LC ($\Delta q < 0.01$ e). Thus, the S_1 shifts of the less stable M^+LC(O2) isomers are substantially smaller. Finally, formation of the M^+–LC bond is accompanied by modest charge transfer from M^+ to LC, which increases with the binding energy of the $M^+\cdots$LC bond (Table 4). For example, q_M = 0.915 and 0.898 e for M^+LC(O4) with M = Cs and Li, respectively. As this bond becomes stronger in the S_1 excited state, the corresponding charge transfer from M^+ to LC increases (q_M = 0.898 and 0.854 e for M = Cs and Li).

It is instructive to compare the properties of M^+LC with those of the related H^+LC ions. While M^+LC(O4) corresponds to a single global minimum, in which M^+ binds in a chelate to the lone pairs of both O4 and N5, the much smaller size of the proton leads to the interaction with either O4 or N5. Both H^+LC minima are very deep (D_0 = 911 and 931 kJ mol^{-1} for O4 and N5) and separated by a large barrier (67 kJ mol^{-1} for N5 → O4 tautomerization). Only the more stable H^+LC(N5) isomer is observed experimentally.[19,23] Because of the stronger bond of H^+ to LC, the computed S_1 red shifts of both H^+LC(N5) and H^+LC(O4) are larger than those of M^+LC(O4), in good agreement with available experimental data for the same ππ* excitation (Fig. 4 and Table 2).

Table 4 Atomic charges (in units of e) of selected atoms of M^+LC(O4) and LC in the S_0 and first ππ* excited singlet state evaluated at the PBE0/cc-pVDZ level using natural bond orbital analysis

	q_M		q_{N5}		q_{O4}		q_{O2}	
	S_0	S_1	S_0	S_1	S_0	S_1	S_0	S_1
Li	0.898	0.854	−0.524	−0.641	−0.728	−0.746	−0.577	−0.559
Na	0.921	0.903	−0.519	−0.617	−0.704	−0.736	−0.570	−0.565
K	0.921	0.904	−0.493	−0.592	−0.704	−0.741	−0.575	−0.568
Rb	0.927	0.911	−0.485	−0.583	−0.698	−0.737	−0.577	−0.570
Cs	0.915	0.898	−0.472	−0.571	−0.699	−0.742	−0.579	−0.571
LC			−0.386	−0.477	−0.565	−0.595	−0.623	−0.615

4. Concluding remarks

The vibronic spectra of M^+LC with M = Li–Cs are recorded by VISPD spectroscopy in a cryogenic ion trap. Significantly, these vibrationally resolved electronic spectra are the first optical spectra of any metalated flavin in the gas phase and thus provide a first impression of the effects of metalation on the intrinsic electronic structure of flavins. The analysis of the rich vibronic spectra using DFT calculations coupled to multi-dimensional FC simulations provides a reliable assignment of the observed band system to the first optically bright ππ* transition ($S_1 \leftarrow S_0$) of the M^+LC(O4) global minima identified previously by IRMPD spectroscopy in a 300 K trap.[20] Large red shifts in the S_1 band origins and intense progressions in the intermolecular $M^+\cdots$LC bend and stretch modes provide a quantitative measure for the substantial increase in the strength of the metal–flavin interaction upon ππ* excitation of M^+LC(O4). The large S_1 red shifts of M^+LC(O4) can be rationalized by the orbitals involved in the ππ* transition and the resulting changes in the charge distribution. The large differences in the energies of the ππ* transition of M^+LC(O4) and M^+LC(O2) demonstrate that the photochemical properties of flavins can indeed drastically be tuned by metal complexation *via* both the type and binding site of the metal ion. The current study may be extended in several directions. First, the IRMPD spectra suggest that the less stable M^+LC(O2) local minima can also be produced by ESI (at least for M = K–Cs).[20] Their predicted S_1 origins are at substantially higher energies compared to those detected here for M^+LC(O4), and we are currently searching for them (Table 2 and Fig. 4). Although they may occur in a spectral range where they may overlap with the second ππ* state of M^+LC(O4), the FC analysis will provide a clear isomer assignment. Second, effects of solvation on the optical properties of metal–flavin complexes may separately be determined by applying the same experimental and computational strategy to microsolvated clusters, in which in a controlled fashion a variable number of polar or nonpolar solvent ligands are attached to the cryogenic flavin ions. In this way, a more complete picture of the photophysical properties of flavins can be derived at the molecular level.

Conflicts of interest

There are no conflicts to declare.

Acknowledgements

This work was supported by Deutsche Forschungsgemeinshaft (DFG, DO 729/6). M. M. is grateful for a senior research

fellowship from the Alexander von Humboldt Foundation (2017-2019). O. D. acknowledges travel support from the World Research Hub Initiative (WRHI) of Tokyo Institute of Technology (Japan). Part of the computations was performed at the Research Center of Computational Chemistry in Okazaki (Japan).

References

1 E. Silva and A. Edwards, *Flavins, Photochemistry, and Photobiology*, RSC Publishing, Cambridge, 2006.
2 K. H. Dudley, P. Hemmerich, F. Müller and A. Ehrenberg, *Helv. Chim. Acta*, 1964, **47**, 1354–1383.
3 P. F. Heelis, *Chem. Soc. Rev.*, 1982, **11**, 15–39.
4 V. Massey, *Biochem. Soc. Trans.*, 2000, **28**, 283–296.
5 W. Buckel and R. K. Thauer, *Chem. Rev.*, 2018, **118**, 3862–3886.
6 W. J. Rutter, *Acta Chem. Scand.*, 1958, **12**, 438–446.
7 I. F. Baarda and D. E. Metzler, *Biochim. Biophys. Acta*, 1961, **50**, 463–471.
8 P. Bamberg and P. Hemmerich, *Helv. Chim. Acta*, 1961, **44**, 1001–1011.
9 F. Müller, P. Hemmerich and A. Ehrenberg, *Eur. J. Biochem.*, 1968, **5**, 158–164.
10 A. W. Varnes, E. L. Wehry and R. B. Dodson, *J. Am. Chem. Soc.*, 1972, **94**, 946–950.
11 J. Lauterwein, P. Hemmerich and J. M. Lhoste, *Inorg. Chem.*, 1975, **14**, 2152–2161.
12 J. Lauterwein, P. Hemmerich and J. M. Lhoste, *Inorg. Chem.*, 1975, **14**, 2161–2168.
13 M. Benecky, T. Y. Yu, K. L. Watters and J. T. McFarland, *Biochim. Biophys. Acta*, 1980, **626**, 197–207.
14 S. Fukuzumi and T. Kojima, *J. Biol. Inorg. Chem.*, 2008, **13**, 321–333.
15 I. Ahmad, Z. Anwar, S. Ahmed, M. A. Sheraz and S. Khattak, *J. Photochem. Photobiol., B*, 2017, **173**, 231–239.
16 E. Sikorska, I. V. Khmelinskii, W. Prukała, S. L. Williams, M. Patel, D. R. Worrall, J. L. Bourdelande, J. Koput and M. Sikorski, *J. Phys. Chem. A*, 2004, **108**, 1501–1508.
17 A. Tyagi and A. Penzkofer, *J. Photochem. Photobiol., A*, 2010, **215**, 108–117.
18 A. Tyagi and A. Penzkofer, *Photochem. Photobiol.*, 2011, **87**, 524–533.
19 J. Langer, A. Günther, S. Seidenbecher, G. Berden, J. Oomens and O. Dopfer, *ChemPhysChem*, 2014, **15**, 2550–2562.
20 A. Günther, P. Nieto, G. Berden, J. Oomens and O. Dopfer, *Phys. Chem. Chem. Phys.*, 2014, **16**, 14161–14171.
21 P. Nieto, A. Günther, G. Berden, J. Oomens and O. Dopfer, *J. Phys. Chem. A*, 2016, **120**, 8297–8308.
22 A. Günther, P. Nieto, D. Müller, A. Sheldrick, D. Gerlich and O. Dopfer, *J. Mol. Spectrosc.*, 2017, **332**, 8–15.
23 A. Sheldrick, D. Müller, A. Günther, P. Nieto and O. Dopfer, *Phys. Chem. Chem. Phys.*, 2018, **20**, 7407–7414.
24 A. Vdovin, A. Slenczka and B. Dick, *Chem. Phys.*, 2013, **422**, 195–203.
25 T. L. Zhang, K. Papson, R. Ochran and D. P. Ridge, *J. Phys. Chem. A*, 2013, **117**, 11136–11141.
26 L. Guyon, T. Tabarin, B. Thuillier, R. Antoine, M. Broyer, V. Boutou, J. P. Wolf and P. Dugourd, *J. Chem. Phys.*, 2008, **128**, 075103.
27 M. H. Stockett, *Phys. Chem. Chem. Phys.*, 2017, **19**, 25829–25833.
28 L. Giacomozzi, C. Kjær, J. Langeland Knudsen, L. H. Andersen, S. Brøndsted Nielsen and M. H. Stockett, *J. Chem. Phys.*, 2018, **148**, 214309.
29 E. Sikorska, I. Khmelinskii, D. Worrall, J. Koput and M. Sikorski, *J. Fluoresc.*, 2004, **14**, 57–64.
30 S. Salzmann and C. M. Marian, *Chem. Phys. Lett.*, 2008, **463**, 400–404.
31 J. Hasegawa, S. Bureekaew and H. Nakatsuji, *J. Photochem. Photobiol., A*, 2007, **189**, 205–210.
32 M. J. Frisch, *et al.*, *GAUSSIAN09, Rev. D.01*, Gaussian, Inc., Wallingford CT, 2009.
33 R. L. Martin, *J. Chem. Phys.*, 2003, **118**, 4775–4777.
34 C. M. Western, *J. Quant. Spectrosc. Radiat. Transfer*, 2017, **186**, 221–242.
35 E. D. Glendening, J. K. Badenhoop, A. E. Reed, J. E. Carpenter, J. A. Bohmann, C. M. Morales, C. R. Landis and F. Weinhold, *NBO 6.0, Theoretical Chemistry*, University of Wisconsin, Madison, 2013.
36 R. D. Shannon, *Acta Crystallogr., Sect. A: Cryst. Phys., Diffr., Theor. Gen. Crystallogr.*, 1976, **32**, 751–767.

